INTERNATIONAL JOURNAL FOR NUMERICAL METHODS IN FLUIDS, VOL. 15, 799–816 (1992)

A FINITE VOLUME APPROACH TO LARGE EDDY SIMULATION OF COMPRESSIBLE, HOMOGENEOUS, ISOTROPIC, DECAYING TURBULENCE

A. W. VREMAN, B. J. GEURTS, J. G. M. KUERTEN AND P. J. ZANDBERGEN

Department of Applied Mathematics, University of Twente, P.O. Box 217, 7500 AE Enschede, The Netherlands

SUMMARY

Large eddy simulation of compressible, homogeneous, isotropic, decaying turbulence in a rectangular box is performed using finite volume techniques. An analysis of the energy spectra obtained from the simulations shows that an agreement with the Kolmogorov law for the inertial range is found only when an appropriate spatial discretization method is used. This agreement is obtained both for a low (0·05) and a moderate (0·6) Mach number when Smagorinsky's subgrid model is employed.

KEY WORDS Large eddy simulation Finite volume methods Compressible turbulence

1. INTRODUCTION

Recently, the large eddy simulation (LES) of compressible, turbulent flows has received considerable attention.[1–3] The large eddy simulation of e.g. a compressible boundary layer is important for aerodynamic applications, since it will contribute to the present understanding of turbulent flow around an aerofoil. In order to handle the complex geometries in such applications, finite volume or finite difference methods are more convenient than spectral methods. However, the question arises whether the discretization errors in finite volume methods will impede their use in large eddy simulations of compressible turbulence. To obtain an answer to this question, it is desirable to consider a simpler type of turbulence first. Therefore, in the study described here, large eddy simulations of compressible, homogeneous, isotropic, decaying turbulence are performed with the use of finite volume methods. This type of turbulence has already been studied in the past, but in most cases with Fourier spectral or pseudospectral methods.[1]

In the evaluation of the results, an essential question is whether the calculated energy spectra agree with the spectrum as predicted by the Kolmogorov theory. Homogeneous, isotropic turbulence is ideally suited for answering this question, since its energy spectra can be easily calculated. Moreover, since no driving force appears in the description, the influence of the numerical scheme on the simulation results will display itself most clearly. It will be shown that finite volume methods are fruitful in the present application, provided that an appropriate spatial discretization of the equations is employed, in which the numerical dissipation in viscous and convective fluxes correctly balance. This does not automatically imply that finite volume methods will be adequate when LES of more complicated flow problems is considered. To the study of homogeneous, isotropic, decaying turbulence, one should add studies of non-homogeneous

0271–2091/92/190799–18$14.00

Received October 1991
Revised April 1992

turbulent flows. For that reason the finite volume approach to the compressible boundary layer and the compressible mixing layer will be the subject of investigation in the near future.

The organization of this paper is as follows. The governing equations are presented in Section 2. In Section 3 the numerical method is described. Section 4 is devoted to the results of semi-incompressible and compressible large eddy simulations. Finally, the conclusions are presented in Section 5.

2. GOVERNING EQUATIONS

The equations governing compressible flow are the well-known Navier–Stokes equations, which represent conservation of mass, momentum and energy. The flow domain Ω considered here is a cube. Each field quantity is periodically continued outside this cube, i.e. we asume periodic boundary conditions. The basic idea behind large eddy simulation is to separate each field variable in Ω into a large-scale and a small-scale quantity using a filtering operation. The large-scale (or filtered) variables are solved explicitly and the small-scale (or fluctuating) quantities are modelled with a subgrid model.

This section presents the filtered Navier–Stokes equations in which the small-scale quantities, which occur when the convective terms are filtered, are modelled by Smagorinsky's subgrid model. The filter operation

$$\bar{f}(\mathbf{x})=\int_{\Omega} G_{\Delta}(\mathbf{x}-\xi)f(\xi)\,\mathrm{d}\xi \tag{1}$$

decomposes a variable f into a large-scale part $\bar{f}$, and a small-scale contribution f', which accounts for the scales not resolved by the filterwidth Δ:

$$f=\bar{f}+f'. \tag{2}$$

A related filter has been introduced by Favre,[4] for use in compressible flow simulations. This is defined by

$$\tilde{f}=\frac{\overline{\rho f}}{\bar{\rho}}, \tag{3}$$

in which ρ is the density. This implies a second decomposition of f:

$$f=\tilde{f}+f''. \tag{4}$$

Applying the filter operation to the Navier–Stokes equations, we find[5,6]

$$\frac{\partial\bar{\rho}}{\partial t}+\frac{\partial}{\partial x_j}(\bar{\rho}\tilde{u}_j)=0, \tag{5}$$

$$\frac{\partial}{\partial t}(\bar{\rho}\tilde{u}_i)+\frac{\partial}{\partial x_j}(\bar{\rho}\tilde{u}_i\tilde{u}_j)=-\frac{\partial\bar{p}}{\partial x_i}+\frac{\partial\bar{\sigma}_{ij}}{\partial x_j}-\frac{\partial\tau_{ij}}{\partial x_j}, \tag{6}$$

$$\frac{\partial}{\partial t}(\hat{E})+\frac{\partial}{\partial x_j}((\hat{E}+\bar{p})\tilde{u}_j)=\frac{\partial}{\partial x_j}(\overline{u_i\sigma_{ij}}-\tilde{u}_i\tau_{ij})-\frac{\partial\bar{Q}_j}{\partial x_j}-\frac{\partial\pi_j}{\partial x_j}-\frac{\partial q_j}{\partial x_j}, \tag{7}$$

where the independent variables t and x_i represent time and the three spatial co-ordinates, respectively. In these equations the summation convention for repeated indices is used. The components of the velocity vector are denoted by u_i, and p is the pressure. Moreover, $\hat{E}$ is the total

energy of the filtered variables, i.e.

$$\hat{E}=\frac{\bar{p}}{\gamma-1}+\tfrac{1}{2}\bar{\rho}\tilde{u}_i\tilde{u}_i. \tag{8}$$

The viscous stress tensor σ_{ij} is defined as

$$\sigma_{ij}=\frac{\mu}{Re}S_{ij}, \tag{9}$$

where μ denotes the dynamic viscosity and S_{ij} the strain rate tensor,

$$S_{ij}=\frac{\partial u_i}{\partial x_j}+\frac{\partial u_j}{\partial x_i}-\tfrac{2}{3}\delta_{ij}\frac{\partial u_k}{\partial x_k}, \tag{10}$$

where δ_{ij} is the Kronecker delta. In addition, Q_j represents the viscous heat flux vector, given by

$$Q_j=-\frac{\mu}{(\gamma-1)RePr\,M_R^2}\frac{\partial T}{\partial x_j}, \tag{11}$$

where T denotes the temperature. The filtered temperature $\tilde{T}$ is related to he filtered density and the filtered pressure by the ideal gas law,

$$\tilde{T}=\gamma M_R^2\frac{\bar{p}}{\bar{\rho}}, \tag{12}$$

and the dynamic viscosity is expressed by Sutherland's law for air,

$$\mu=T^{3/2}\frac{1+C}{T+C}. \tag{13}$$

The equations have been made dimensionless by introducing a reference length L (the length of the side of Ω), a reference velocity u_R, a reference density ρ_R, a reference temperature T_R and a reference viscosity μ_R. (The reference value of the velocity is equal to the L_2-norm of the initial velocity field. The same scaling is adopted for density, temperature and viscosity.) In addition, the constants C, γ (being the ratio of the specific heats C_p and C_v) and the Prandtl number Pr are given the following values:[5]

$$C=0{\cdot}4, \tag{14}$$

$$\gamma=1{\cdot}4, \tag{15}$$

$$Pr=0{\cdot}72. \tag{16}$$

The Reynolds number $Re=\rho_R u_R L/\mu_R$ and reference Mach number $M_R=u_R/a_R$, where a_R is a reference value for the speed of sound, will be varied in the simulations.

The three terms τ_{ij}, π_j and q_j are the subgrid quantities resulting from the non-linearity of the convective terms. Subgrid quantities resulting from the non-linearity of σ_{ij}, Q_j and μ are neglected.[5] The three subgrid quantities which are taken into account, are defined by

$$\tau_{ij}=\bar{\rho}(\widetilde{u_iu_j}-\tilde{u}_i\tilde{u}_j), \tag{17}$$

$$\pi_j=\overline{pu_j}-\bar{p}\tilde{u}_j \tag{18}$$

and

$$q_j=\frac{\bar{\rho}}{(\gamma-1)\gamma M_R^2}(\widetilde{Tu_j}-\tilde{T}\tilde{u}_j). \tag{19}$$

The first term τ_{ij} is modelled by

$$-\tau_{ij}=\bar{\rho}\nu_t\tilde{S}_{ij}-\tfrac{2}{3}\delta_{ij}\bar{\rho}k, \tag{20}$$

where k represents the trace of τ_{ij} divided by 2. The second term on the right-hand side of equation (20) is incorporated into the pressure term, whereas the eddy viscosity ν_t in the first term is prescribed by Smagorinsky's model:

$$\nu_t=C_S^2\Delta^2\left(\tilde{S}_{ij}\frac{\partial\tilde{u}_i}{\partial x_j}\right), \tag{21}$$

where we have chosen $C_S=0{\cdot}2$ and Δ equal to the grid size h. This model is the most commonly used subgrid model in large eddy simulation of incompressible flow. When it is used for compressible flow, equation (21) takes into account some compressiblity effects because the strain rate tensor S_{ij} depends on the divergence of the velocity. The eddy viscosity as given in equation (21) has indeed been used for simulations of the weakly compressible mixing layer.[2]

The two other subgrid terms, which occur in the energy equation, are modelled with an eddy diffusivity μ_t/Pr_t. In Reference 7 Pr_t was calculated for compressible isotropic turbulence. Values ranging from 0·4 to 0·9 were found. In the present study we set $Pr_t=0{\cdot}9$. Simulations performed with other settings of Pr_t, e.g. $Pr_t=Pr$, do not show any significant differences.

The theoretical basis of LES is not very sound. The derivation of Smagorinsky's subgrid model requires several assumptions which can be questioned since they are only based on dimensional analysis. Moreover, in general, the spatial derivatives and the filtering operator do not commute close to the boundaries, as supposed in the derivation of (5–7). We illustrate this with a simple one-dimensional example. Consider a function f defined on an interval $\Omega=[a, b]$, then

$$\overline{\frac{\partial f}{\partial x}}(x)-\frac{\partial\bar{f}}{\partial x}(x)=G(x-b)f(b)-G(x-a)f(a). \tag{22}$$

The expression does not necessarily vanish for an arbitrary boundary condition, if the support of G is larger than the distance from x to a or to b. A convenient extrapolation of f outside the domain can be constructed such that $\bar{f}$ satisfies the same boundary conditions as f. In general, the lack of commutation of filtering operator and spatial derivatives close to the boundaries, however, may imply that the boundary conditions for $\bar{f}$ are to be taken different from those for f. It is not at all clear how this approach can be generalized to arbitrary geometries in two or three dimensions.

3. NUMERICAL METHODS

In this section we concentrate on the numerical approximations of the spatial derivatives and their representations in Fourier space. First, however, we briefly sketch the time integration method.

The time-stepping method which we adopt is an explicit 4-stage Runge–Kutta method. When we consider the scalar differential equation $du/dt=f(u)$, this Runge–Kutta method performs within one time step

$$u^{(j)}=u^{(0)}+\beta_j\Delta t f(u^{(j-1)}), \tag{23}$$

with $u^{(0)}=u(t)$ and $u(t+\Delta t)=u^{(4)}$. With the coefficients $\beta_1=1/4$, $\beta_2=1/3$, $\beta_3=1/2$ and $\beta_4=1$ this yields a second-order accurate time integration method. A stability analysis shows that this method is not too dissipative.[8] If the time step Δt is adequately restricted, the dissipation due to

Table I. The difference operators D_j with the corresponding l_j.

Operator	Name	l_j
D_1	Cell vertex trapezoidal	$l_1=\frac{\sin(k_1 h)}{h}(1+\cos(k_2 h)(1+\cos(k_3 h))/4$
D_2	Vertex centered	$l_2=\frac{\sin(k_1 h)}{h}$
D_3	Cell vertex Simpson	$l_3=\frac{\sin(k_1 h)}{h}(2+\cos(k_2 h))(2+\cos(k_3 h))/9$
D_4	Fourth order	$l_4=\frac{4\sin(k_1 h)}{3h}-\frac{\sin(2k_1 h)}{6h}$
D_5	Staggered central difference	$l_5=\frac{\sin(k_1 h/2)}{h/2}\cos(k_2 h/2)\cos(k_3 h/2)$

the Runge–Kutta scheme can be neglected when compared to effects related to the spatial derivatives.

Usually, the time integration method is not an important issue in the discussion of LES. The spatial discretization however, plays a more dominant role. We will compare in total six different numerical methods based on finite volume techniques. In order to describe these methods, we introduce five difference operators $D_1, \ldots, D_5$ representing different options for the numerical approximation of $\partial/\partial x_1$. It is sufficient to consider only derivatives with respect to x_1; derivatives with respect to x_2 and x_3 are treated in a similar manner. Table I introduces the operators D_j and their names. All these operators are second-order accurate except for D_4, which is fourth-order accurate. For convenience we describe these operators in a two-dimensional setting; extension to three dimensions is straightforward. In all cases we treat homogeneous, isotropic turbulence on a uniform grid with the same number of grid points (N) in each direction. Since the non-dimensionalized length of the cube is 1, the mesh distance h equals $1/N$. The operator D_j is evaluated at vertex (m, n). The operators D_1, D_2, D_3 and D_5 can be symbolically expressed as

$$\frac{S_{\text{right}}-S_{\text{left}}}{\delta}. \tag{24}$$

in which $\delta=2h$, except for D_5, where $\delta=h$. Since S_{left} follows from S_{right} and the symmetry of each operator, we will only pay attention to S_{right}. In the case of D_1, the trapezoidal rule over the vertices $(m+1, n-1)$, $(m+1, n)$ and $(m+1, n+1)$ is used for the calculation of S_{right}. In contrast, in D_2 the midpoint rule is used, so that S_{right} is based on vertex $(m+1, n)$ only. D_3 is similar to D_1, but with the Simpson integration rule used instead of the trapezoidal rule. In the case of D_5, S_{right} is dcalculated using the cell centres $(m+1/2, n-1/2)$ and $(m+1/2, n+1/2)$. This difference operator is, therefore, appropriates when it is applied to the viscous stress tensor and the heat flux, since the discrete version of these two quantities (again with use of D_5) can be defined in cell centres quite naturally. The control volume of the three operators D_1, D_2 and D_3 equals $8h^3$, whereas the control volume related to D_5 equals h_3. Finally, the opertor D_4 is the fourth-order accurate finite difference method that uses the vertices $(m-2, n)$, $(m-1, n)$, $(m+1, n)$ and $(m+2, n)$.

Next, the action of the difference operator D_j on a Fourier mode will be discussed in order to describe the structure of the operator in more detail. We write

$$D_j(e^{ik\cdot x})=i\,l_j\,e^{ik\cdot x}, \tag{25}$$

where $\mathbf{k}=[k_1, k_2, k_3]^T$ denotes the wave vector and l_j is the approximation of k_1 obtained with method D_j. The expressions for l_j can be found in Table I. We call D_j dissipative for wave number $\mathbf{k}$ if $|l_j(\mathbf{k})| \leq |k_1|$.

The values k_i can be expressed as $2\pi n$ with $n=-N/2+1, \ldots, N/2$. Thus, we see that for $|k_1|$ close to πN (the small-scale components), the staggered operator D_5 is less dissipative than D_2. Further, D_3 is always more dissipative than D_2 but less dissipative than D_1. Summarizing, we have $|l_1(\mathbf{k})| \leq |l_3(\mathbf{k})| \leq |l_2(\mathbf{k})| \leq |l_5(\mathbf{k})| \leq |k_1|$, in case $k_2=k_3=0$. The operator D_4 is somewhat more complicated and cannot be ordered in the above estimates. All operators are dissipative on a single Fourier mode, but their dissipative character varies.

It is convenient to separate the space derivative terms in equations (5)–(7) into two classes of terms: the convective terms and the viscous terms. The convective terms are identified as the divergence terms on the left-hand side of (5)–(7) and the pressure gradient term on the right-hand side. These terms contain only first-order spatial derivatives. The remaining (viscous) terms contain second-order derivatives. In what follows we refer to a combination of two schemes as a *method*. In Table II we present several such methods. The convective terms can be described with one operator D_c. The viscous terms have to be described with two operators $D_v D_\sigma$. D_σ represents the derivatives within the stress tensor σ_{ij} and the heat flux Q_j, while D_v stands for the divergence applied to the stress tensor and the heat flux.

Note that for uniform rectangular grids an explicit finite volume method corresponds with a second-order accurate spatial discretization of the governing equations, if we divide the discrete equations by the control volume. The discrete surface integrals appear to be discrete divergence terms. This is the reason why a finite volume method can be represented by a difference operator D_j. Method A, for example, is a finite volume method in which the convective fluxes are integrated over a control volume consisting of eight cells, while the dissipative fluxes are integrated over a smaller control volume consisting of one single staggered cell. In methods E and F the control volume for the convective and viscous terms is the same. Since D_1–D_5 are all purely symmetric, the discrete equations still conserve mass, momentum and energy.

Method A[9] has been successfully employed in the ISNaS solvers for simulations of compressible, turbulent flow around aerodynamic bodies, based on the Reynolds-averaged Navier–Stokes equations. In Section 4 this method will be shown to be too dissipative for fluctuations corresponding to large wave numbers. Guided by this, the numerical approximations of the convective and/or viscous terms can be improved fruitfully in such a way that the fluctuations corresponding to large wave numbers are properly represented. It is essential that the convective and viscous terms are treated with schemes that assign the proper dissipation to each of these terms, so that the physics is represented accurately even on a coarse grid. With the Fourier representations l_j of the operators D_j, we can explain in part the qualitative relation between the evolution of the tail of the energy spectrum and the numerical method. As an example, method E, in which the viscous terms are treated with $D_3 D_2$, will damp the high wave number contributions

Table II. Six different numerical methods, built with D_1–D_5

Method	Convective terms		Viscous terms	
A	D_1	cell vertex trapezoidal	$D_5 D_5$	staggered central difference
B	D_2	vertex centered	$D_5 D_5$	staggered central difference
C	D_4	fourth order	$D_5 D_5$	staggered central difference
D	D_3	cell vertex Simpson	$D_5 D_5$	staggered central difference
E	D_3	cell vertex Simpson	$D_3 D_2$	cell vertex Simpson
F	D_1	cell vertex trapezoidal	$D_1 D_2$	cell vertex trapezoidal

less than method A, in which the viscous terms are treated with $D_5 D_5$. This is due to the fact that for $|k|$ near (but smaller than) πN the following inequality holds: $l_3 l_2 \ll l_5 l_5$. If the high wave number contributions are damped less, the tail of the energy spectrum will be higher. Turning to method B e.g. we observe that the only difference with method A is in the treatment of the convective fluxes. Since $l_2 \leqslant l_1$, the numerical dissipation in the convective fluxes is lower in method B and, hence, the spectrum will be higher. The discussion of the results in Section 4 will be mainly based on similar arguments. We are presently studying more rigorous approaches.

The initialization of the variables is done with the algorithm presented by Erlebacher *et al.*[10] In this approach randomly generated fields for density, velocity and temperature are adjusted in such a way that they satisfy a prescribed autocorrelation spectrum.The autocorrelation spectrum of the velocity for example (usually called energy spectrum) is defined by

$$E(k, t) = \int_{|\mathbf{k}|=k} |\hat{\mathbf{u}}(\mathbf{k}, t)^2 \, \mathrm{d}S. \tag{26}$$

The initial spectrum that is prescribed can be written as

$$E_{\text{init}}(k) = k^4 \mathrm{e}^{-2k^2/k_{\text{peak}}^2}. \tag{27}$$

It attains its maximum at k_{peak}, allowing a direct control over the 'dominant' large-scale structures initially. Moreover, the compressibility factor χ (the fraction of the kinetic energy that corresponds to the acoustic component of the velocity[10] and the rms values of density and temperature are prescribed.

4. RESULTS

The results of calculations at a low Mach number ($M_R = 0{\cdot}05$) and of calculations at a higher Mach number are presented ($M_R = 0{\cdot}6$).

Semi-incompressible simulations

To compare the different numerical methods given in Table II, we perform a number of semi-incompressible ($M_R = 0{\cdot}05$) simulations with parameters as given in Table III. The peak wave number k_{peak} determines the initial scale of the large eddies, having approximately a characteristic length $2\pi/k_{\text{peak}}$. Thus, $k_{\text{peak}} = 6\pi$ indicates that we have approximately three large eddies in one direction. In order to see the generation of higher Fourier modes, there ought to be a reasonable distance between k_{peak} and $k_{\max} = \pi N$ (which is the maximum length of a component

Table III. Parameters determining the initial fields

Parameters	Semi-incompressible simulations	Compressible simulations
Grid	21^3	48^3
Time step	0·001	0·004
Reference Mach number, M_R	0·05	0·6
Taylor Reynolds number, Re_λ	40	50
Peak wave number	6π	12π
Initial compresibility, χ	0·0	0·1
Initial rms, ρ	0·0	0·1
Initial rms, T	0·0	0·1

of the wave vector). On the other hand, when k_{peak} is too small, the large eddies will be strongly influenced by the periodic boundary conditions. Re_λ is the Reynolds number based on the Taylor microscale λ.[11] The microscale Renolds number $Re_\lambda = 40$ corresponds with $Re_L = 583$, which is the Reynolds number based on L, the length of the box. Initially, λ is 0·11, while the eddy turnover time initially equals 0·20. Each simulation was performed for at least two eddy turnover times.

We will evaluate the results with two criteria: *energy spectra* and *skewness*. According to Kolmogorov,[12] there exists an inertial range of the energy spectrum $E(k)$, where $E(k) \propto k^{-5/3}$. Although a strict agreement with the Kolmogorov theory may require a very high resolution, an agreement for low resolutions was observed in literature (see, for example, Reference 3 where simulations on a 20^3 grid were performed with a finite difference method). The skewness tensor of velocity derivatives is defined by

$$\mathrm{Sk}_{ij} = \frac{\langle (\partial u_i/\partial u_j)^3 \rangle}{\langle (\partial u_i/\partial x_j)^2 \rangle^{3/2}} . \tag{28}$$

We will concentrate on Sk_{11} in the sequel. Accordings to References [13 and 12], experimental values of the skewness found in grid turbulence are of the order of $-0{\cdot}4$. Direct simulations give values of approximately $-0{\cdot}5$ at $Re_\lambda = 40$.[1] The skewness is initially close to zero and, hence, a minimal requirement for an 'acceptable' method is that the skewness at least becomes and remains negative during the simulation.

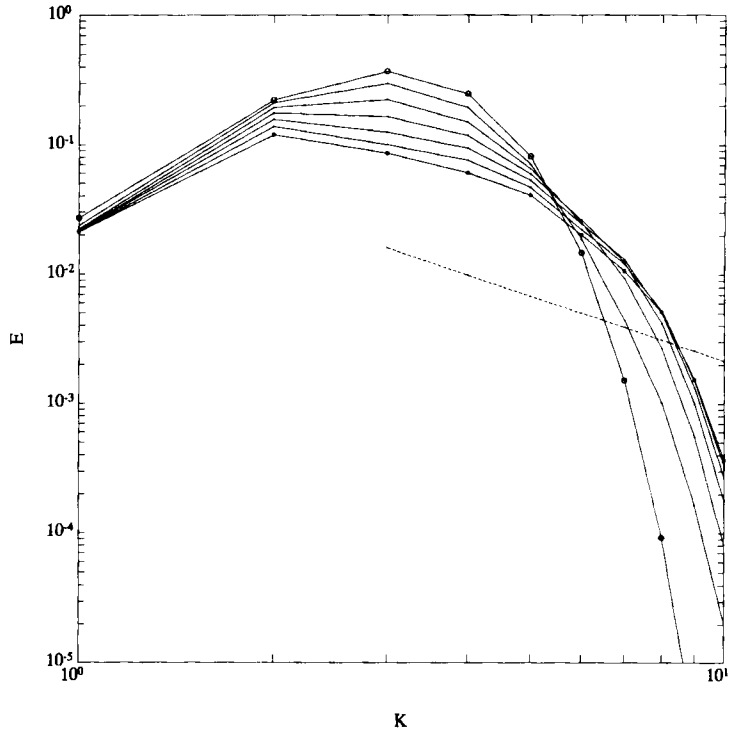

Figure 1. The evolution of the energy spectrum E, obtained with LES on a 21^3 grid for $M_R = 0{\cdot}05$, calculated with method A. Time interval between two successive curves: 0·06; o: initial spectrum; *: spectrum at $t = 0{\cdot}36$; dashed line: Kolmogorov's $-5/3$ law

Figure 1 shows the energy spectrum using method A (which forms our point of reference). The skewness evolves to $-0{\cdot}3$ approximately, in reasonable agreement with the results mentioned above. We observe that the peak shifts towards lower wave numbers, in agreement with literature; see e.g. Reference 12. For high wave numbers, however, the spectrum does not agree with the Kolmogorov theory; it is too steep. Decreasing the Smagorinsky constant does not give better results. Thus, the reason is likely to be found in the numerical method. The tail of the spectrum depends sensitively on the balance between convective and dissipative terms for high wave numbers. Method A is too dissipative. Hence, we may change this method along two different lines:

1. Increase the generation of high wave number contributions. The energy transfer to higher wave numbers is largely due to the convective terms for they contain the highest degree of non-linearity. By altering the discretization of the convective terms, we can increase l_c for higher wave numbers and, thus, stimulate the generation of high wave number fluctuations.
2. Decrease the dissipation of high wave number contributions. This can be done by changing the schemes used for the viscous terms, i.e. adopting schemes with lower $l_v l_\sigma$ for high wave numbers.

These two options are clearly represented in the methods presented in Table II. Both options will produce an energy spectrum which is less steep for high wave numbers than the spectrum obtained with method A. First we consider the first option and change the convective terms, such that the numerical dissipation decreases.

In method B the convective terms are treated with a scheme that is much less dissipative ($l_2 \geq l_1$), especially for high wave numbers. However, Figure 2 shows that in this case the damping is insufficient; the spectrum 'blows up'. A higher Smagorinsky constant ($C_s = 0{\cdot}34$) gives a better spectrum, but a cusp at high $|\mathbf{k}|$ remains. The skewness is inadequately predicted; it becomes positive during the simulations. Changes in the discretization of the convective fluxes have a large effect on the simulation results. This is further clarified in method C where the discretization of the convective terms is a fourth-order method. Both energy spectrum and skewness have the same qualitative behaviour as in method B. The generation of high wave number contributions is even more rapid, since $l_4 \geq l_2$ for $0 \leq k_1 \leq \pi N$.

In method D a second-order scheme for the convective terms, based upon the Simpson integration rule was introduced. The spectrum is similar to Figure 1, only the tail is slightly higher. This is clearly the effect of $l_3 \geq l_1$ for high wave numbers; method D is less dissipative than method A, but nevertheless still too dissipative. The skewness is as in method A.

Thus, it appears that it is not sufficient to change the scheme for the convective terms only. Methods A, B, C and D all have one thing in common: they treat the convective terms essentially different from the viscous terms. In all four methods (A–D) l_c is quite different from $l_v = l_5$ and $l_\sigma = l_5$, causing a wrong balance between convective and dissipative terms, especially for wave numbers near k_{max}.

Therefore, in method E the scheme for the viscous terms was altered, according to the second option mentioned, making the viscous dissipation smaller for high wave numbers, since $l_3 l_2 \leq l_5 l_5$. The resulting spectrum, shown in Figure 3, seems to be better than all spectra obtained before. A close agreement with the Kolmogorov law is obtained. Many more time steps (approximately 300) have to be performed compared to the simulation with method A, before the tail of the spectrum does not further increase. Most simulations are stopped when the tail of the spectrum is observed to decrease. From that time on a possible 'blow up' of the spectrum is highly unlikely. This is illustrated by a performance of the simulation with method E for a longer time (twice the time covered by Figure 3). We note that after having obtained the $-5/3$ slope the spectrum slowly

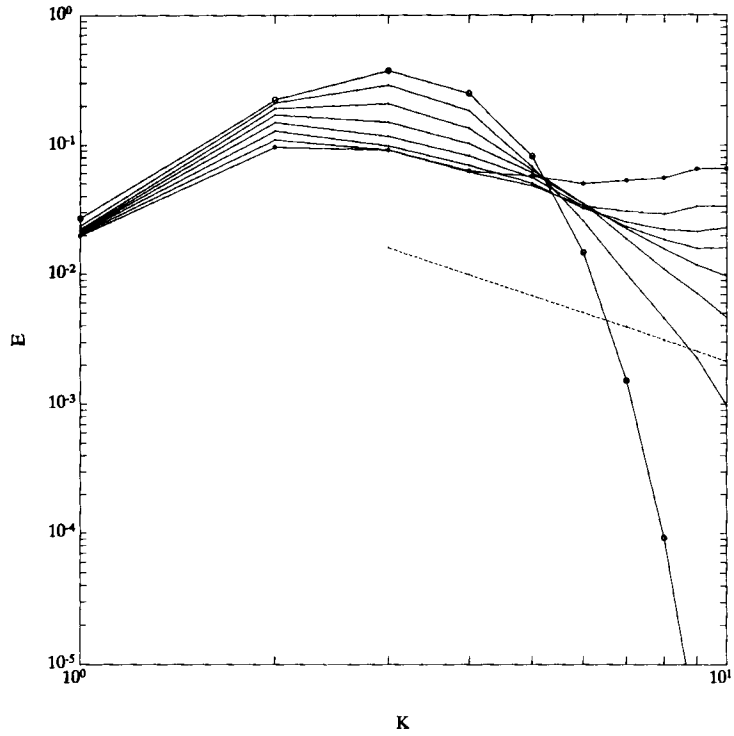

Figure 2. The evolution of the energy spectrum E, obtained with method B. Parameters as in Figure 1.

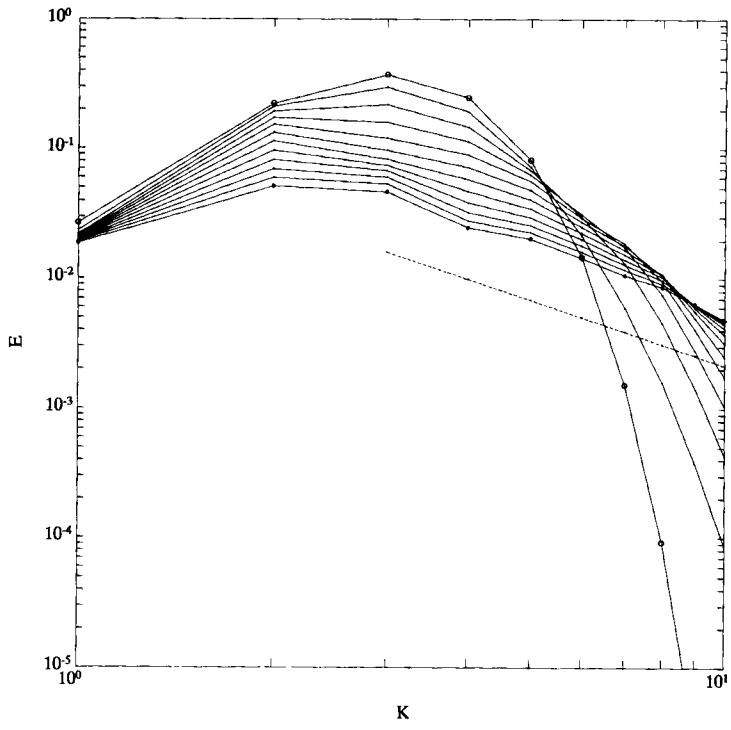

Figure 3. The evolution of the energy spectrum E, obtained with method E. Parameters as in Figure 1

evolves into different shape, since it decreases faster at low wave numbers than at high wave numbers. Thus, a cusp occurs, which might be a shortcoming of the model. Smagorinsky's model is an eddy viscosity model and, thus, mainly dissipative. The cusp shows that the combination of method E and the Smagorinsky model still needs a mechanism that redistributes energy from small to large scales. An energy backscatter might be a solution. The skewness obtained with method E is reasonably accurate. It is comparable to the skewness obtained with methods A and D. Thus, the simulation with method E results in agreement with both Kolmogorov's law and the skewness requirement. The only shortcoming of simulations with method E lies in the very long time behavior of the energy spectrum, as has been described.

In order to investigate another method, which the viscous terms are treated in the same way as the convective terms, method F is introduced. Method F differs from method E only in the integration rule being used; trapezoidal in F, instead of Simpson in E. Method F is more dissipative than method E and the tail of the corresponding spectrum is a bit too steep. The skewness is slightly worse as compared to method E (where it was close to $-0{\cdot}3$, here close to $-0{\cdot}2$).

Resuming, we observe that method A appears too dissipative for high wave numbers. The results can be improved by the implementation of less dissipative discretization schemes for the convective terms (methods B, C and D), but the improvement is insufficient. Treating the convective terms as in method A and only changing the treatment of the viscous fluxes is found insufficient as well (method F). However, we observe that method E, in which the treatment of both convective and viscous terms have been changed with respect to our reference method A, represents the spectrum and skewness reasonably well. A correct 'balance' between inertial and viscous forces at high wave numbers is obtained with this choice. Table IV summarizes the results.

So, different discretization schemes yield both qualitatively and quantitatively different energy spectra. This gives the following view on LES on a coarse grid with schemes that exhibit only second-order spatial accuracy: not only the subgrid model, but the truncation error as well plays an important role in the reproduction of the Kolmogorov law. This is confirmed by a second observation: an increase of resolution does not always yield a better energy spectrum. When the resolution is increased from 21^3 to 48^3, the tail of the energy spectrum is too steep, for each method used. However, the energy spectra are improved, if resolution and k_{peak} are increased simultaneously. Note that an increase of k_{peak} implies a shift of the initially dominant structure to smaller scales, hence reducing the effects of the periodic boundary conditions.

As a further clarification, we introduce the energy transfer function $T(k, t)$. For incompressible flow the relation between $T(k, t)$ and $E(k)$ is given by

$$T(k, t)=\left(\frac{\partial}{\partial t}+2\nu k^2\right)E(k), \tag{29}$$

Table IV. Skewnesss and spectra for six different numerical methods, where + indicates good and − bad agreement with theoretically expected results

Method	Skewness	Spectrum	Corresponding figure
A	+	−	1
B	−	+/−	2
C	−	+/−	
D	+	−	
E	+	+	3
F	+/−	+/−	

where ν is the kinematic viscosity.[12] We use the same expression to define $T(k, t)$ in the compressible case. With this definition the integral of $T(k, t)$ over all k-values is no longer equal to zero for compressible flow, since the decay of the total kinetic energy is not only affected by viscosity, but also by the product of the pressure and the velocity divergence. Moreover, the viscosity for compressible flow is not constant. Therefore, we take an averaged value of the laminar and eddy- viscosity in (29). As a result $T(k, t)$ as given by (29) does not represent transfer of energy only. However, at low Mach number, compressibility is small and $T(k, t)$ predominantly represents transfer of energy so that it can quite reliably be used for illustrating the energy transfer in the various methods. In Figure 4 $T(k, t)$ is plotted for simulations with methods A, B and E. $T(k, t)$ being positive for high wave numbers indicates the tendency for the energy to Acascade from large to small scales. The figure reveals that in method A there is almost no energy transfer at subgrid-scale level, while in method B the transfer at subgrid-scale level dominates. Method E shows a transfer of energy at subgrid-scale level, which seems to approach a limiting value. The correlation with the corresponding spectra is immediate. Method A has a tail which is too steep, in agreement with the high wave number behaviour of T. The dominant energy transfer at subgrid scales in method B is clearly related to the 'blow up' of the spectrum. Finally, in method E an adequate balance is obtained with T approaching a non-zero limiting value.

As a final test for the semi-incompressible simulations with finite volume methods, we investigate the influence of the initial conditions. We observe that after a transient period of, say, one eddy turnover time different initial conditions give rise to approximately the same spectrum and skewness.

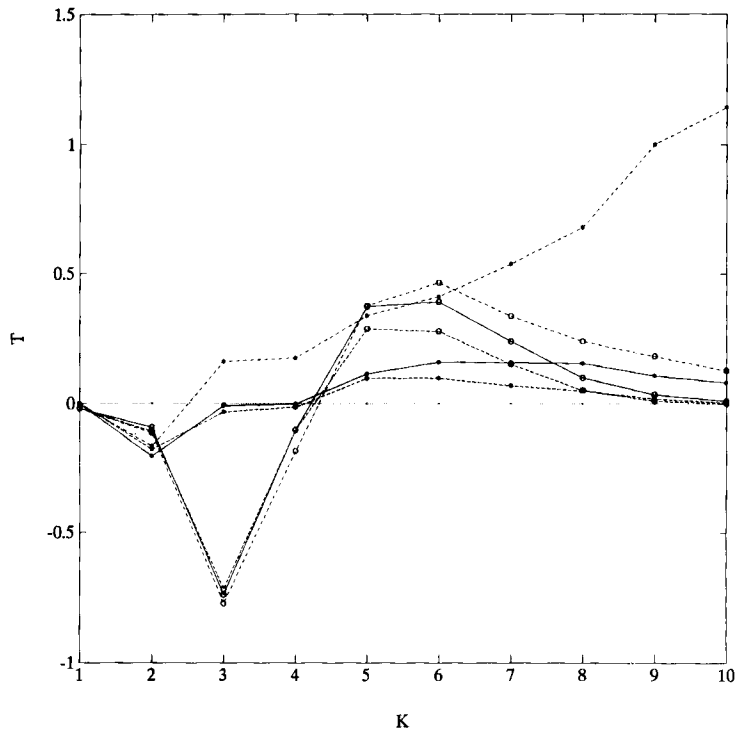

Figure 4. The energy transfer function T, obtained with LES on a 21^3 grid for $M_R = 0{\cdot}05$. Dashed: method A; dashdot: method B; solid: method E; o: transfer at $t = 0{\cdot}09$; *: transfer at $t = 0{\cdot}36$

All methods presented so far are second-order accurate in space. We also implemented higher-order methods in order to study the effects of the accuracy of the spatial discretization. In case we use a full fourth-order method, i.e. $D_c = D_v = D_\sigma = D_4$ with the same parameter settings, the spectrum does not agree with Kolmogorov's law and resembles qualitatively Figure 2. Treating the spatial derivatives with a pseudospectral method, results in a spectrum with a much too steep tail, compared to the $-5/3$-law, although it is less steep than the spectrum in Figure 1. Qualitatively, the spectrum obtained with the pseudospectral method resembles those presented in Reference14, in which three-dimensional compressible turbulence is simulated with direct and large eddy simulations.

Compressible simulations

Next we consider simulations at a Mach number of 0·6. Moreover, initial compressibility has been included, i.e. χ, and the rms values of ρ and T are initially not equal to zero. The parameters are given in Table III. The simulations were performed for approximately four eddy turnover times, i.e. $0 \leq t \leq 0{\cdot}4$. The higher Mach number, i.e. higher compressibility, was found not to alter the dependence of the time evolution of the energy spectrum on the numerical method. Therefore, we restrict ourselves to the presentation of results obtained with method E.

In Figure 5 the evolution of the energy spectrum is shown, whereas Figure 6 represents the autocorrelation spectrum of the density. An agreement with Kolmogorov's law can be observed in both quantities though for the density autocorrelation spectrum this is not as clear as for the

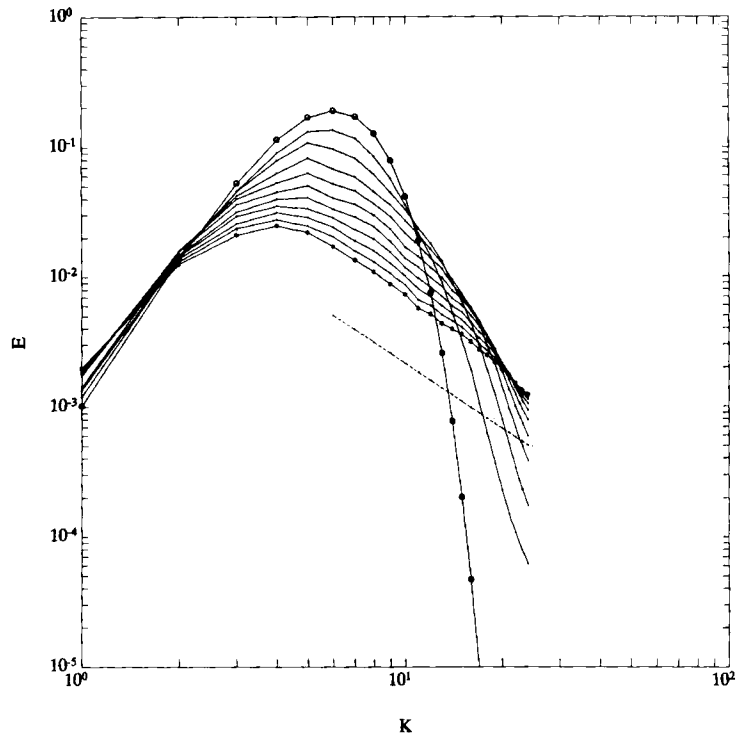

Figure 5. The evolution of the energy spectrum E, obtained with LES on a 48^3 grid for $M_R = 0{\cdot}6$. Time interval between two successive curves: 0·04; o: initial spectrum; *: spectrum at $t = 0{\cdot}40$; dashed line: Kolmogorov's $-5/3$ law

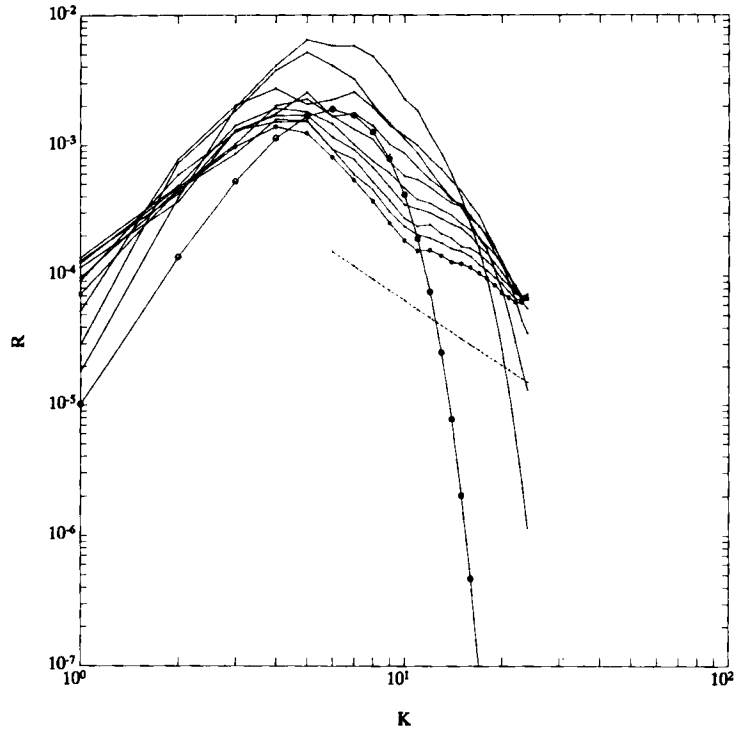

Figure 6. The evolution of the density autocorrelation spectrum R, obtained with LES on a 48^3 grid for $M_R=0{\cdot}6$. Parameters as in Figure 4

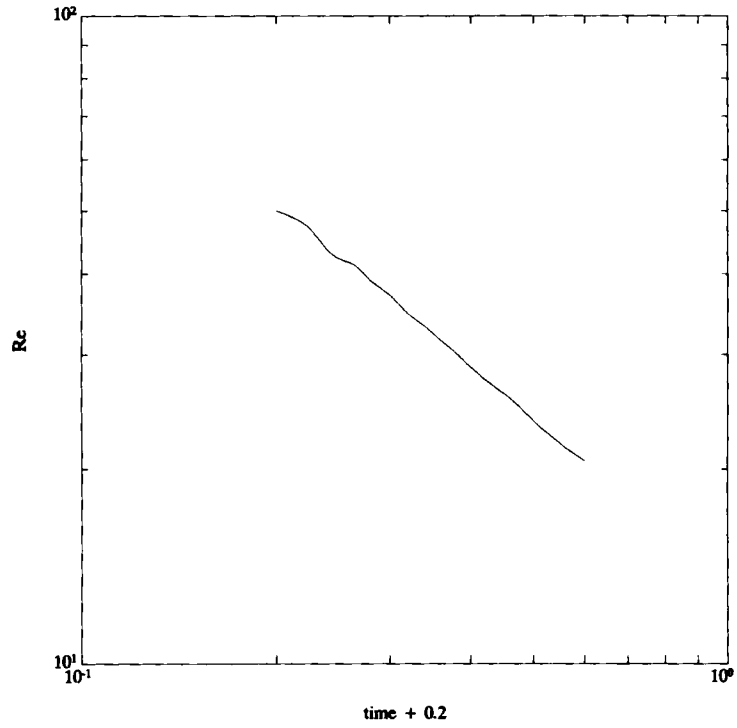

Figure 7. Time history of the Reynolds number based on the Taylor microscale λ, obtained with LES on a 48^3 grid for $M_R=0{\cdot}6$

energy spectrum. Figure 6 shows that the rms of the density heavily fluctuates. The Taylor microscale λ is initially 0·05. After a transient period in which λ decreases (until $t=0\cdot2$), λ starts to increase slowly, as observed e.g. in Reference 1, where the results were obtained with a spectral method. The Reynolds number based on the Taylor microscale decreases from 50 to 20. The decay is smooth and regular and it exhibits a power-law dependence of the form $Re_\lambda \propto (t+\alpha)^m$ with $\alpha \approx 0\cdot2$ and $m=-0\cdot86$ (Figure 7). The von Karman–Howarth/Batchelor–Townsend theory predicts $m=-0\cdot75$.[13] The constant computational Reynolds number, which is based on the length of the box is equal to 1660. Thus, the eddy viscosity (with initial mean $0\cdot64\times10^{-3}$ and rms $0\cdot22\times10^{-3}$) is of the same order of magnitude as μ/Re. The skewness lies indeed between $-0\cdot4$ and $-0\cdot5$ for a moment, but increases afterwards as shown in Figure 8. The skewness keeps fluctuating around $-0\cdot2$ for $t>0\cdot4$. The values $-0\cdot4$ and $-0\cdot5$ relate to incompressible flow; compressibility seems to affect the skewness,[15] i.e. increased fluctuations are observed and it takes a longer time before it reaches a stationary level.

Next, we discuss the behavior of the compressibility parameter χ. The theory presented in Reference 10 predicts that the asymptotic value of χ increases when M_R decreases. This theory concerns two-dimensional turbulence and is restricted to low Mach numbers ($M_R \approx 0\cdot1$). Nevertheless, we observe in Figure 9 a similar behaviour of χ: the asymptotic value of χ increases when M_R decreases. The initial value of χ is the same in these cases.

The next two figures are both taken from the data at a two-dimensional section of the cube, namely face $z=0$. Figure 10 shows the density at $t=0$, whereas Figure 11 presents the density at

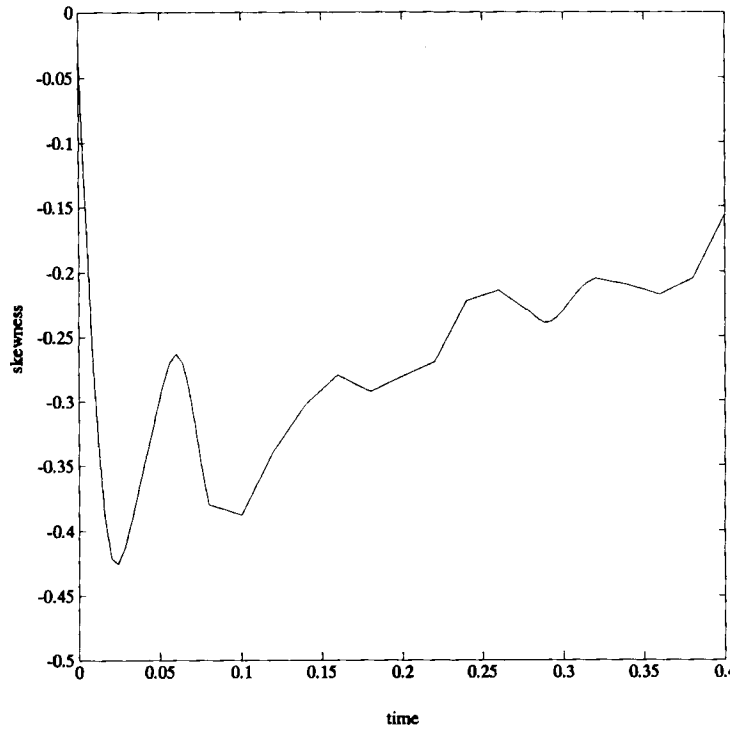

Figure 8. Time history of the skewness component Sk_{11} obtained with LES on a 48^3 grid for $M_R=0\cdot6$

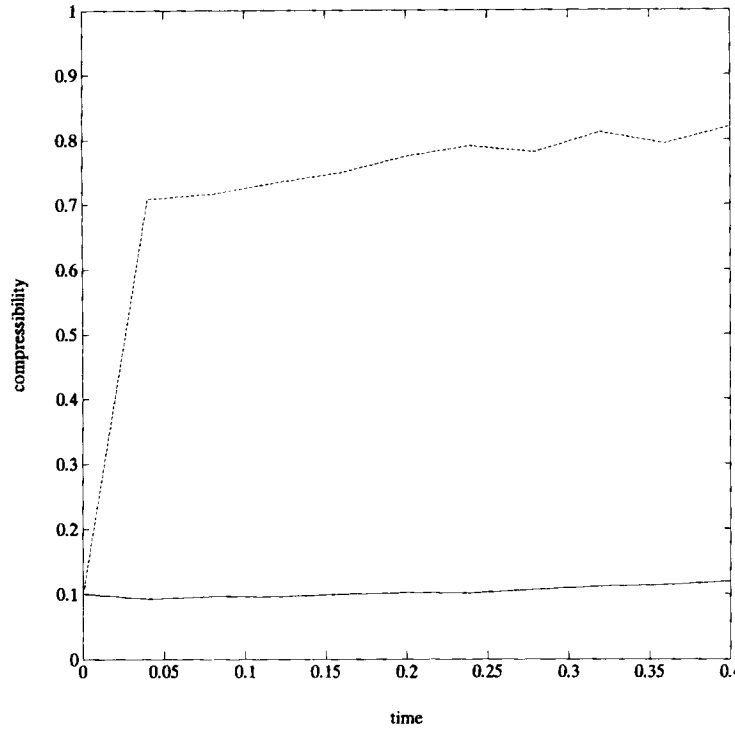

Figure 9. Time history of the compressibility factor χ for $M_R = 0{\cdot}05$ (dashed) and $M_R = 0{\cdot}6$ (solid), obtained with LES on a 48^3 grid

$t = 0{\cdot}3$ at which time the flow satisfied the Kolmogorov law. Comparing these two figures, we notice that higher Fourier modes have been introduced at $t = 0{\cdot}3$, corresponding to steeper gradients and more small-scale fluctuations. Of course, this is what we would expect. Moreover, when similar plots are made for the pressure, a strong correlation of density and pressure is observed.

The results presented here were all obtained with Smagorinsky's model (21). Other subgrid models have been studied as well and it appears that the influence of the subgrid model is not always so dominant. Simulations with the structure function eddy viscosity model as proposed by Normand and Lesieur[3] and even a simulation with a constant eddy viscosity yield essentially the same spectra as the simulations with Smagorinsky's model. Thus, the spectrum does not seems to validate the subgrid model, but only the constant in front of the subgrid model (in these cases)! To validate the subgrid model itself we considered the correlation of subgrid stresses with direct simulation results (cf. Reference 1). We found a correlation coefficient around 0·3 for Smagorinsky's model and the structure function model, whereas the correlation coefficient for the subgrid model corresponding to a constant eddy viscosity, turned out to be somewhat smaller (around 0·2).

5. CONCLUSIONS

We have shown the importance of an appropriate spatial discretization method in achieving the desired agreement with the Kolmogorov law for the inertial range. Energy spectra are sensitive to

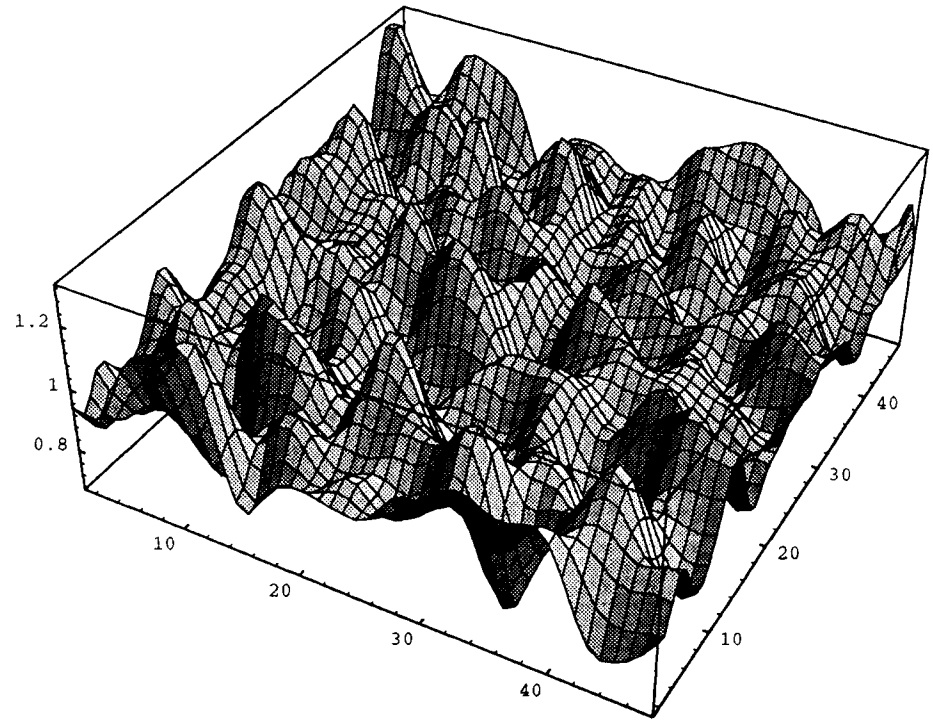

Figure 10. The density $\rho(x, y, z=0)$ at $t=0$, with ρ along the vertical axes, obtained with LES on a 48^3 grid

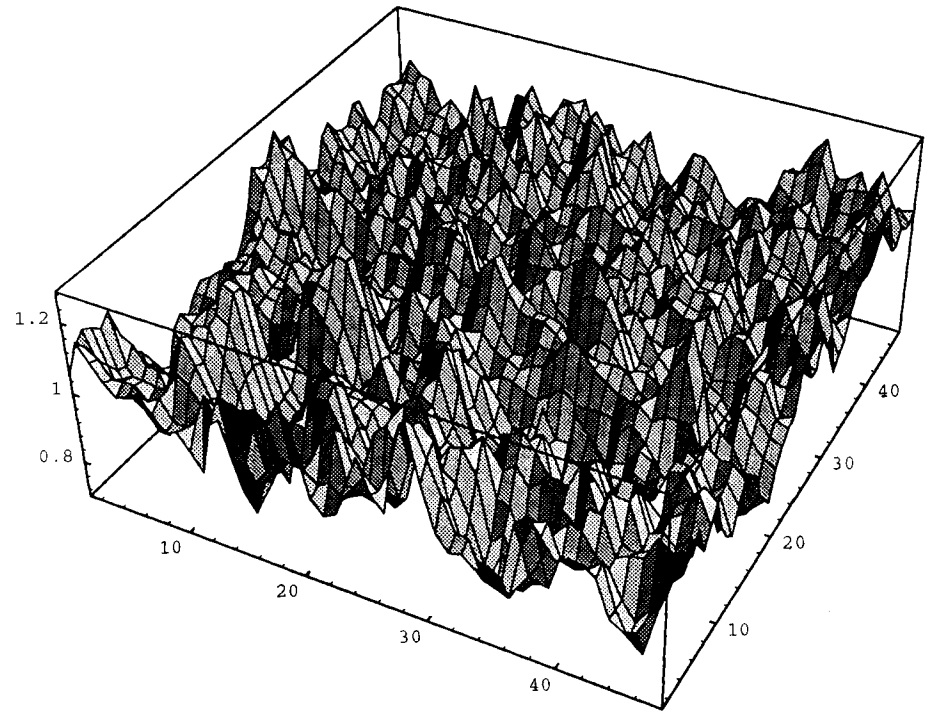

Figure 11. The density $\rho(x, y, z=0)$ at $t=0{\cdot}3$, with ρ along the vertical axes, obtained with LES on a 48^3 grid

the type of spatial discretization, especially when we use grids with low resolution. Satisfactory results are obtained even on a coarse grid, when the convective and viscous terms are both treated with the Simpson cell vertex method, although some problems remain even with this method when simulations with very long integration times are performed. A subgrid model is necessary in order to give sufficient damping, but the type of the subgrid model is less important. Only the spatially averaged value of the eddy viscosity must be adequately represented. Even with a constant eddy viscosity one may generate adequate spectra and integral quantities. A first comparison with direct simulation results did not prove the superiority of a particular subgrid model. In addition, Smagorinsky's subgrid model produces reasonably good results for simulations at a moderate Mach number. We must stress, of course, that this concerns homogeneous isotropic turbulence.

As a general conclusion we can state that this study shows that finite volume methods can be used to perform large eddy simulations of compressible turbulence, but that one has to be careful in the choice of the spatial discretization method.

ACKNOWLEDGEMENTS

The development of the ISNaS solver was sponsered by the Stichting Nationale Computerfaciliteiten (National Computing Facilities Foundation, NCF) and financially supported by the Nederlandse Organisatie van Wetenschappelijk Onderzoek (Netherlands Organization for Scientific Research, NWO). We are thankful to the referees for several useful comments.

REFERENCES

1. G. Erlebacher, M. Y. Hussaini, C. G. Speziale and T. A. Zang, 'Toward the large eddy simulations of compressible turbulent flows', *ICASE Report No. 87-20*, NASA Langley Research Centre, 1987.
2. C. E. Leith, 'Stochastic backscatter in a subgrid-scale model: Plane shear mixing layer', *Phys. Fluids A*, **2**, 297–299 (1990).
3. X. Normand and M. Lesieur, 'Direct and large-eddy simulations of transition in the compressible boundary layer', *Theoret. Computational Fluid Dyn.*, **3**, 231–252 (1992).
4. A. Favre, 'Turbulence: space–time statistical properties and behavior in supersonic flows', *Phys. Fluids*, **26**, 2851–2863 (1983).
5. F. J. Brandsma, 'Mathematical and physics aspects of simulations based on the Navier–Stokes equations', *ISNaS 88.08.024/NLR TP 89069 L*, 1989.
6. K. Squires and O. Zeman, 'On the subgrid-scale modeling of compressible turbulence', *Proc. Summer Program 1990*, Stanford, 1990.
7. P. Moin, K. Squires, W. Cabot and S. Lee, 'A dynamic subgrid-scale model for compressible turbulence and scalar transport', CTR Manuscript 124, Stanford University, 1991.
8. A. Jameson, 'Transonic flow calculations', *MAE-Report 1651*, Princeton University, 1983.
9. J. G. M. Kuerten, 'Numerical definition document for the ISNaS time-explicit flow solver', Memorandum No. 934, University of Twente, 1991.
10. G. Erlebacher, M. Y. Hussaini, H. O. Kreiss and S. Sarkar, 'The analysis and simulation of compressible turbulence', *Theoret. Computational Fluid Dyn.*, **2**, 73–95 (1990).
11. H. Tennekes and J. L. Lumley, *A First Course in Turbulence*, The MIT Press, Cambridge, 1972.
12. M. Lesieur, *Turbulence in Fluids*, Kluwer Academic Publishers, Dordrecht, 1987.
13. S. Tavoularis, J. C. Bennett and S. Corrsin, 'Velocity-derivative skewness in small Reynolds number, nearly isotropic decaying turbulence', *J. Fluid Mech.*, **88**, 63–69 (1978).
14. T. A. Zang, R. B. Dahlburg and J. P. Dahlburg, 'Direct and large-eddy simulations of three-dimensional compressible Navier–Stokes turbulence', *Phys. Fluids A*, **4**, 127–140 (1992).
15. S. Lee, S. K. Kele and P. Moin, 'Eddy-shocklets in decaying compressible turbulence', CTR Manuscript 117, Stanford University, 1990.